J Nanopart Res (2019) 21: 47
https://doi.org/10.1007/s11051-019-4489-2

RESEARCH PAPER

Microwave-assisted synthesis and photothermal conversion of $Cu_{2-x}Se$ hollow structure

Zejia Zhao · Guozhi Jia · Yanling Liu · Qiurui Zhang · Na Wang

Received: 4 October 2018 / Accepted: 14 February 2019 / Published online: 2 March 2019

Abstract The $Cu_{2-x}Se$ nanostructure is rapidly synthesized via one-pot microwave-assisted method. Excellent aqueous dispersion $Cu_{2-x}Se$ hollow structures with an average diameter 160–180 nm and a shell thickness 11.3 nm are obtained successfully. The formation mechanism of the hollow structure is discussed in detail. The NPs exhibits a superior photostability and photothermal conversion efficiency (48%) owing to its unique cavity effect and LSPR property.

Keywords Nanocrystalline materials · Thermal properties · $Cu_{2-x}Se$ · Microwave-assisted

Introduction

The photothermal conversion of nanomaterials has attracted extensive attention owing to its potential application in nanoscale heat sources (Bernal et al. 2018), biological imaging (Park et al. 2017), and photothermal therapy (Jia et al. 2016a; Song et al. 2016). The noble metal is a typical photothermal conversion material based on resonant oscillation of their free electrons in the presence of light (Hanus et al. 2017). The intense interaction between light and noble metal electron can change transition electron process through localized surface plasmon resonance (LSPR), which can result in rapidly converting light into heat. The various nanomaterials, such as MoS_2 nanoflakes (Kong et al. 2017) and carbon nanotubes (Wang et al. 2017), have also been shown to generate sufficient heat by NIR optical illumination. In more cases, treatment needs to be synchronized in a variety of forms, including photothermal and drug therapy. This may require the photothermal conversion materials with more functions, not only with the optimum size range, strong absorption capacity, and adequate biocompatibility. It can be essential that the new type of photothermal materials need be further investigated in urgent need for medical research and photothermal therapy development. The copper chalcogenides semiconductors have been extensively recognized due to biocompatible and low toxicity. Recently, the creation and utilization of vacancies in $Cu_{2-x}Se$ hollow nanospheres have attracted extensive attention owing to the great potential in energy conversion and storage such as photovoltaics, thermoelectrics, photoacoustic (PA) imaging, and photothermal therapy (PTT) (Liu and Swihart 2014; Chen et al. 2015a, b; Han et al. 2015). The hollow nanostructures can act as an extremely vehicles for enclosing multi-functional active materials such as proteins, enzymes, and DNA (Yu et al. 2018; Ni et al. 2017). For example, in terms of minimally invasive photothermal therapy, $Cu_{2-x}Se$ hollow structure as a trigger for targeted cell death brings out local heating under the light excitation. Especially, the trace selenide belongs to the promising bio-friendly element due to their low cytotoxicity (Rayman 2005; Xu et al. 2018; Jia et al. 2015). The nanoscale copper deficient $Cu_{2-x}Se$ has been successfully applied as

Z. Zhao · G. Jia (✉) · Y. Liu · Q. Zhang · N. Wang
School of Science, Tianjin Chengjian University, Tianjin 300384, China
e-mail: jiaguozhi@tcu.edu.cn

efficient photothermal transducers for PA imaging and PTT, because of the strong LSPR from the vacancy in NIR range (Hessel et al. 2011; Liu et al. 2013). By the strong LSPR in $Cu_{2-x}Se$ hollow nanoparticles, the vacancies also offer space sites for designing them into multicomponent structures through various doping means, which contribute to a broad spectrum for tuning their inherent electronic, optical, and magnetic properties for diverse applications (Han et al. 2014; Jiang et al. 2017; Chen et al. 2016). Therefore, the design and preparation of the copper chalcogenides semiconductors have gained a lot of interest due to their applications in various areas.

Here, we report that the $Cu_{2-x}Se$ hollow nanostructures are successfully synthesized by microwave-assisted method. The $Cu_{2-x}Se$ hollow nanostructures possess not only high photothermal conversion efficiency in 980-nm wavelength, but also excellent photostability, which can be attributed to the nanostructures with strong LSPR and special hollow structures. The investigation further suggests that the $Cu_{2-x}Se$ hollow nanostructures could be used in nanoscale heat sources and cancer therapy, which pave a new way for the expansive future applications.

Experiments

$Cu_{2-x}Se$ hollow spheres (NPs) are prepared by a one-pot microwave-assisted method. In brief, the synthesis process of $Cu_{2-x}Se$ is described as follows.

A typical experimental apparatus used for the microwave heating is shown in Fig .1. The apparatus installs a condenser tube through holes in the top and thermocouple connecting directly to temperature indicator and a magnetic stirrer plate coated with Teflon in the bottom of the oven. A thermocouple made of an optical fiber, which is not damaged under microwave irradiation. These reagents of $Cu_{2-x}Se$ including $CuCl_2{\cdot}2H_2O$ (0.3970 g), PVP powers (0.4666 g), Na_2SeO_3 powder (0.2014 g), and NaOH (0.2495 g) are added into ethylene glycol (60 ml). The mixture is stirred for 30 min and then heated to 180 °C for approximately 60 min in a 100-mL three-neck flask equipped with thermal couple and reflux condenser in the microwave oven. The reagent solution is irradiated by microwave in a continuous wave mode. After 60 min, opening microwave oven and the mixture is allowed to cool down to room temperature naturally. The product is centrifuged at the speed of 8000 rpm for 30 min and washed three times with deionized water and ethyl alcohol, respectively. The powder is then collected and dried overnight.

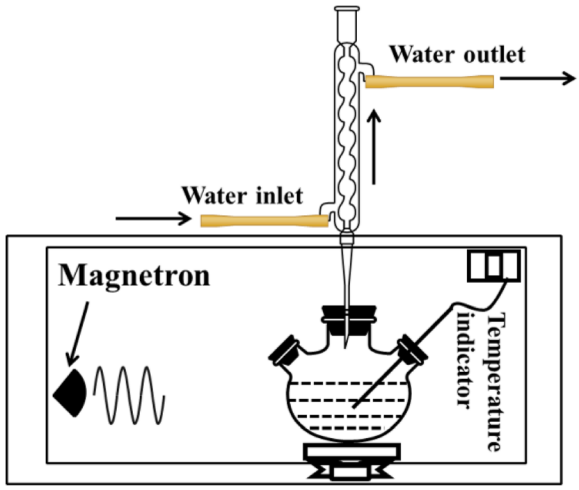

Fig. 1 Apparatus used for the microwave-assisted synthesis of $Cu_{2-x}Se$ nanostructures

The as-prepared $Cu_{2-x}Se$ nanostructure powders are dispersed in aqueous solution for photothermal measurement. A quartz cuvette interior (1.0 mL) containing $Cu_{2-x}Se$ aqueous solutions of various concentrations is irradiated by a 980-nm NIR laser. The laser power is calibrated accurately using an operable optical power meter. Infrared thermometer with accuracy of ± 0.1 °C is applied to test the temperature on the $Cu_{2-x}Se$ aqueous dispersion.

Results and discussion

The morphology of the as-prepared samples is analyzed by transmission electron microscopy (TEM) using a JEOL microscope operated at 200 kV, and showed in Fig. 2a.

It can clearly see that the nanostructures are spherical hollow structures due to the typical electron transparent in the middle area as well as shade on the edge. The result of HRTEM, the selected area electron diffraction (SAED), and the fast Fourier transforms (FFT) pattern are showed in Fig. 2b, c, and d, respectively. The lattice with inter planar spacing of 0.20 nm and 0.33 nm is corresponding to the (220) and (111) planes of cubic berzelianite, respectively. Figure 2e shows the statistical size distribution of diameter of NPs mainly concentrates in 165 nm and can be fitted as the typical Gaussian

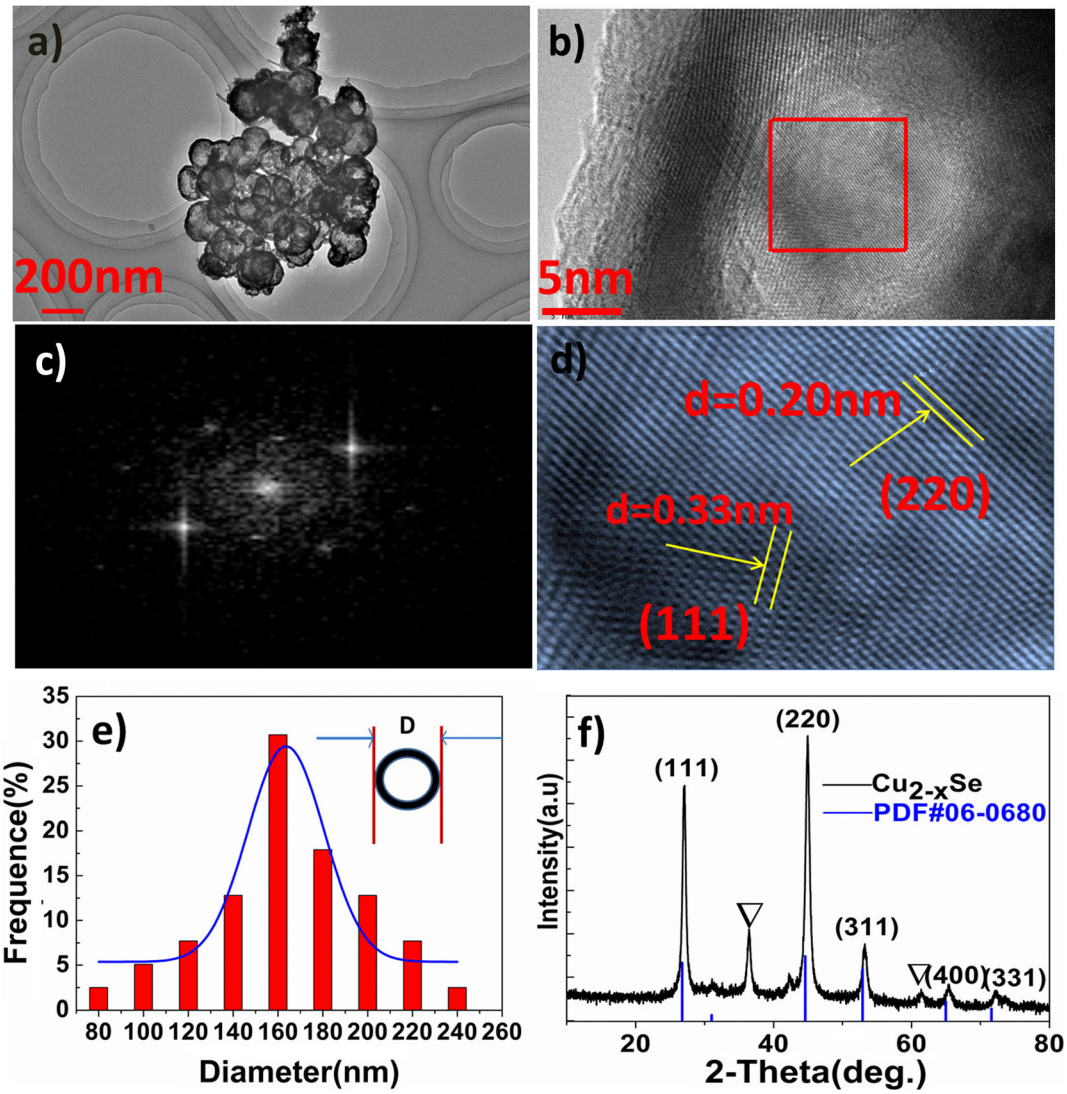

Fig. 2 **a** TEM image showing stack of $Cu_{2-x}Se$ NPs. **b** HRTEM image of NPs. **c** The fast Fourier transform (FFT) of the electron diffraction pattern of NPs. **d** The inversing transformed of Fourier transform to obtain the filtered lattice fringes. **e** The size distribution for NPs. **f** X-ray diffraction pattern of NPs

distribution, which can mainly be ascribed to the rapid and uniform growth of NPs. The crystal structure of NPs is further analyzed by powder X-ray diffraction (XRD) and recorded by a Shimadzu XRD-7000 with Cu-K radiation in Fig. 2f. The XRD peaks indicate that the primary five peaks including (111), (220), (311), (400), and (331) are basically assigned to the standard characteristic peaks of cube berzelianite ($Cu_{2-x}Se$, JCPDS Card No. 06–0680). The average size of NP_S is calculated about 11.3 nm according to Debye-Scherrer formula (Liao et al. 2001) and well agreement with the result obtained by the HRTEM. The sample $Cu_{2-x}Se$ prepared by the assistant-microwave is nonstoichiometric rather than stoichiometric $Cu_{2-x}Se$, which can be ascribed to the phase transformation from $Cu_{2-x}Se$ to $Cu_{2-x}Se$ during the reaction process (Zhang et al. 2016). The lattice constant $a = 5.817$ Å calculated is well agreement with the reported value (Ingole et al. 2009). It can be clearly found that the five main peaks depended on the lattice parameters have slightly moved to higher angles due to the existing of deficient. The other two peaks (400) and (331) can arise from the nonstoichiometric copper-

deficient of $Cu_{2-x}Se$. The rapid reaction can induce Se residue in as-prepared powders.

As TEM does not offer clear 3D images of the obtained $Cu_{2-x}Se$ hollow nanoparticles, the typical field-emission scanning electron microscope (FESEM) with energy dispersive X-ray spectroscopy (EDX) is utilized to investigate the overall appearance of such products by FESEM-6700 field-emission microscope. Figure 3a is the SEM image of the $Cu_{2-x}Se$ hollow nanoparticles, showing that the as-prepared $Cu_{2-x}Se$ hollow nanoparticles are regular hollow spheres. Furthermore, broken particles clearly show the existence of hollow interior, and the SEM image of high magnification indicates that spheres' surface are made up of some small $Cu_{2-x}Se$ nanoparticles in Fig. 3b. Such observations are consistent with the TEM. The size distribution of the $Cu_{2-x}Se$ hollow nanoparticles is estimated from SEM images analysis of $Cu_{2-x}Se$ hollow nanoparticles and the nanoparticles with main size of 170 nm.

The size distribution of $Cu_{2-x}Se$ nanoparticles from 80 to 200 nm are obtained by Zetersizer NanoPlus, while the main concentration of these nanoparticle size is 160–180 nm in Fig. 3c. The nanoparticles' dispersions solutions exhibited a dark green ligand-stabilized solution due to the light scattering of the nanoparticles. Some of their TEM photographs are shown in Fig. 2e, in which the average nanoparticle sizes are approximately 160 nm. These values agreed roughly with those determined by Zetersizer NanoPlus. This implied that a handful of $Cu_{2-x}Se$ nanoparticles can gradually reunite with time increasing. The concentration/stiochiometry of Cu in nanoparticles can be decided by EDX. The EDX analysis of $Cu_{2-x}Se$ composite showed the existence of Se and Cu elements. The atomic ratio of Cu/Se in the $Cu_{2-x}Se$ is about 1.9:1 by EDX analysis, which is different from the theoretical ratio value of 2:1 that calculated from the amount of $CuCl_2 \cdot 2H_2O$ and Na_2SeO_3 powder in the preparation. The result is accord with XRD analysis.

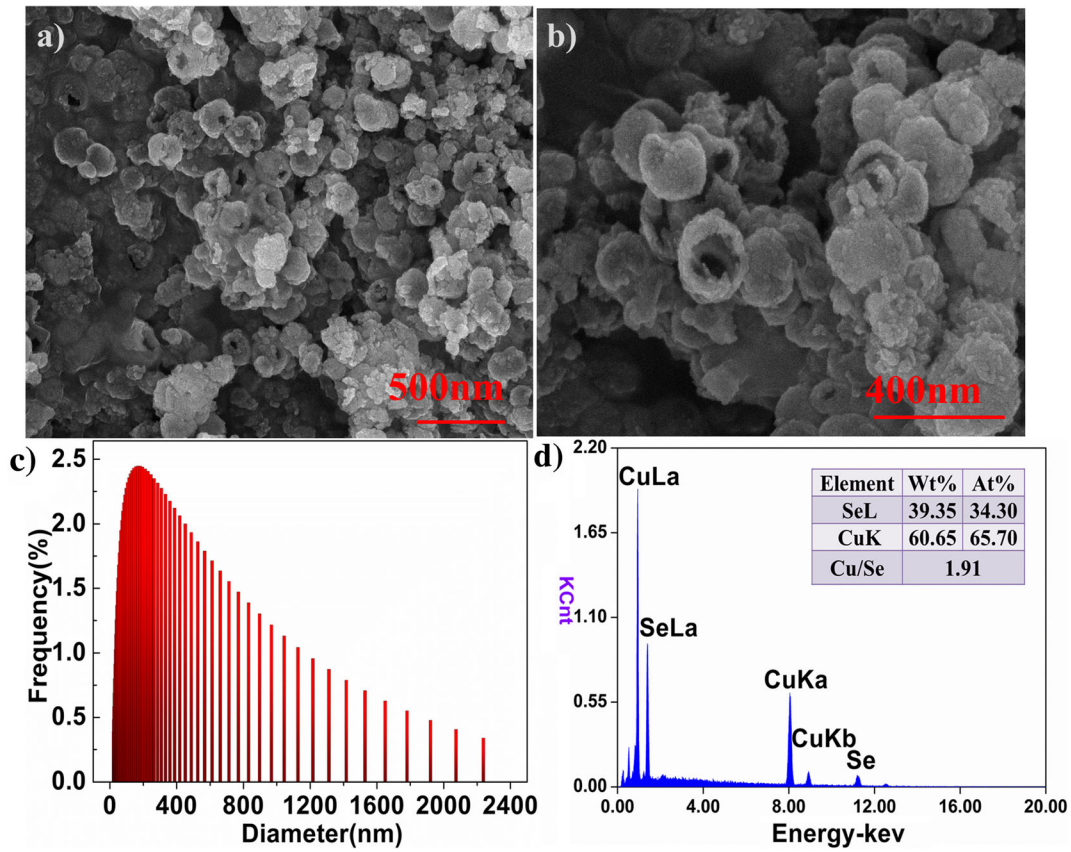

Fig. 3 **a**, **b** SEM image of obtained $Cu_{2-x}Se$ hollow spheres. **c** The size distribution for NPs. **d** The corresponding EDX spectra of $Cu_{2-x}Se$ composite

In order to clearly understand the formation process of the hollow structure, it can be essential to analyze the reaction process and kinetic mechanism (Jia et al. 2013; Chang et al. 2005). The formation of $Cu_{2-x}Se$ NPs hollow structures by microwave irradiation is built on the profound overheating in microwave boiled solvents (Ahmad et al. 2017). This effect is particularly significant in the presence of a large amount of ions. The overheating can result in accelerating the reduction of resultant precursors and the nucleation of the clusters. And in this initial, the reactants may also strongly interact with microwave radiation to produce very high temperatures, enhancing the reduction of ions. $Cu_{2-x}Se$ NPs can be formed by reduction of Na_2SeO_3 with ethylene glycol assistance according to the following reactions:

$$Cu^{2+}\text{–PVP} + OH^- \rightarrow Cu(OH)_2\text{–PVP} \quad (1)$$

$$CH_2OH\text{–}CH_2OH \rightarrow CH_3CHO + H_2O \quad (2)$$

$$SeO_3^{2-} + CH_2OH\text{–}CH_2OH \rightarrow Se^{2-} + CH_3COCOCH_3 + H^+ \quad (3)$$

$$Cu^{2+}\text{–PVP} + Se^{2-} \rightarrow CuSe\text{–PVP} \quad (4)$$

$$CuSe\text{–PVP} + Cu^{2+}\text{–PVP} + Se^{2-} \rightarrow Cu_2Se\text{–PVP} + Se \quad (5)$$

$$Cu(OH)_2\text{–PVP} + CH_3CHO \rightarrow Cu_2O\text{–PVP} + CH_3COCOCH_3 + H^+ \quad (6)$$

$$Cu_2Se\text{–PVP} + Cu_2O\text{–PVP} + H_2O + O_2 + Se^{2-} \rightarrow Cu_{2-x}Se\text{–PVP} + OH^- \quad (7)$$

The reaction process is corresponded to the previously related literature (Cao et al. 2006; Zhang et al. 2017; Tsuji et al. 2005). The specific reactive process is discussed in detail as follows. Before these reagents of the microwave heating, the mixture performs blue color due to the formation of $Cu(OH)_2$. During the process of the microwave heating, the reaction process and kinetic mechanism of $Cu_{2-x}Se$ hollow nanoparticles can be described as a two-step procedure. Cu_2O as a template is firstly reacted with Se^{2-} in appropriate reaction condition owing to $Cu_{2-x}Se$ with the lower solubility (K_{sp}) than Cu_2O, and $Cu_{2-x}Se$ layer is formed on the surface of Cu_2O particles (Cao et al. 2006). This thin layer consisted of many small $Cu_{2-x}Se$ nuclei, which are formed by the reaction between copper ions produced from Cu_2O particles and selenium icons provided by selenium source, and the process can be terminated until the depletion of free copper ions during the dissolution-precipitation process. Then, the $Cu_{2-x}Se$ nanoparticles start to grow on the Cu_2O particles surface based on "Ostwald ripening." The supply of copper ions can be viewed as copper ions migrating from particle interior to the surface duo to the Kirkendall effect (Yu et al. 2018; Yin et al. 2004). During the total reaction processing, copper ions are further moved outward and selenium ions into inward, eventually, Cu_2O templates are converted into $Cu_{2-x}Se$ in the presence of OH^-. The above process results in forming of $Cu_{2-x}Se$ hollow nanoparticles.

As shown in Fig. 4a, the color of the solution gradually changed from yellow-green to black with increasing concentration of $Cu_{2-x}Se$ NPs, indicating the $Cu_{2-x}Se$ NPs are well water-dispersed. The UV-Vis-NIR absorption spectra of $Cu_{2-x}Se$ NPs aqueous solutions are measured by a Perkin Lambda spectrophotometer, as showed in Fig. 4b. It can be clearly seen that the absorbance increases apparently (from 800 to 1100 nm), showing strong LSPR in the NIR region owing to high density vacancies induced by the copper deficiency (Yu et al. 2018).

Nine hundred eighty nanometers of NIR laser with a power density of 1.6 w/cm^2 is delivered through a quartz cuvette containing 1 mL $Cu_{2-x}Se$ NPs aqueous solution to measure photothermal conversion during the NIR laser ON/OFF. It can be showed that the temperature of pure water is increased by less than 5 °C in Fig. 5a. The temperature of aqueous dispersion can rapidly increase by 30 °C in 10 min with the increasing of the NPs concentration, and then nearly saturates with further increases of concentration, which can be attributed to a fast heat loss at relatively high temperatures. The NIR photostability of $Cu_{2-x}Se$ NPs is further investigated; it can clearly be seen that five cycles of the NIR laser ON/OFF are employed, the temperature elevation almost is the same, shown in Fig. 5b, which indicates as-prepared

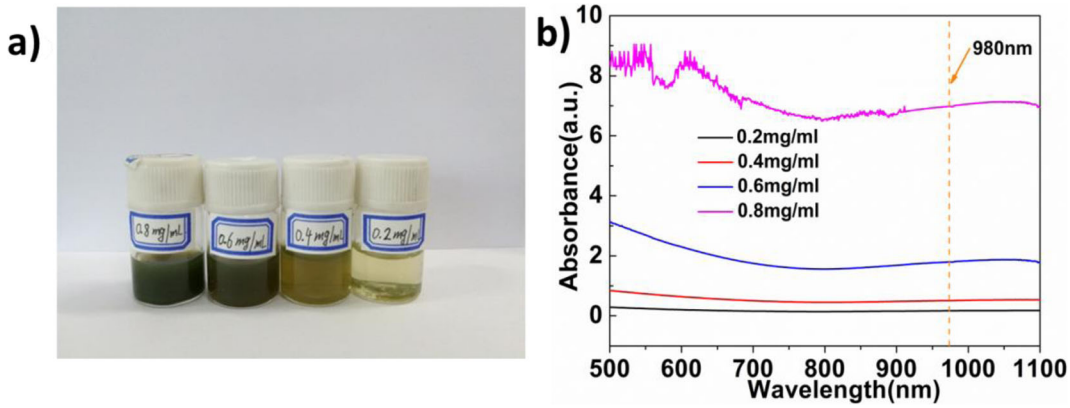

Fig. 4 **a** Photograph of $Cu_{2-x}Se$ aqueous solution. **b** Ultraviolet-Visible (UV-Vis)-NIR absorbance spectra of various concentrations $Cu_{2-x}Se$ aqueous solution

NPs with excellent photostability. The photothermal conversion efficiency and heat transfer time constant can be determined based on the energy balance equation (Jia et al. 2015, 2016b). The thermal equilibrium time constant for heat transfer time determined as the negative reciprocal slope of $\ln(\theta)$ vs.t using temperature versus time data recorded during the cooling of the solution (Fig. 5c). The time constant of the samples is calculated to be 163.2, 182.3187.2, and 180.4 s for the concentrations 0.2, 0.4, 0.6, and 0.8 mg/ml, respectively.

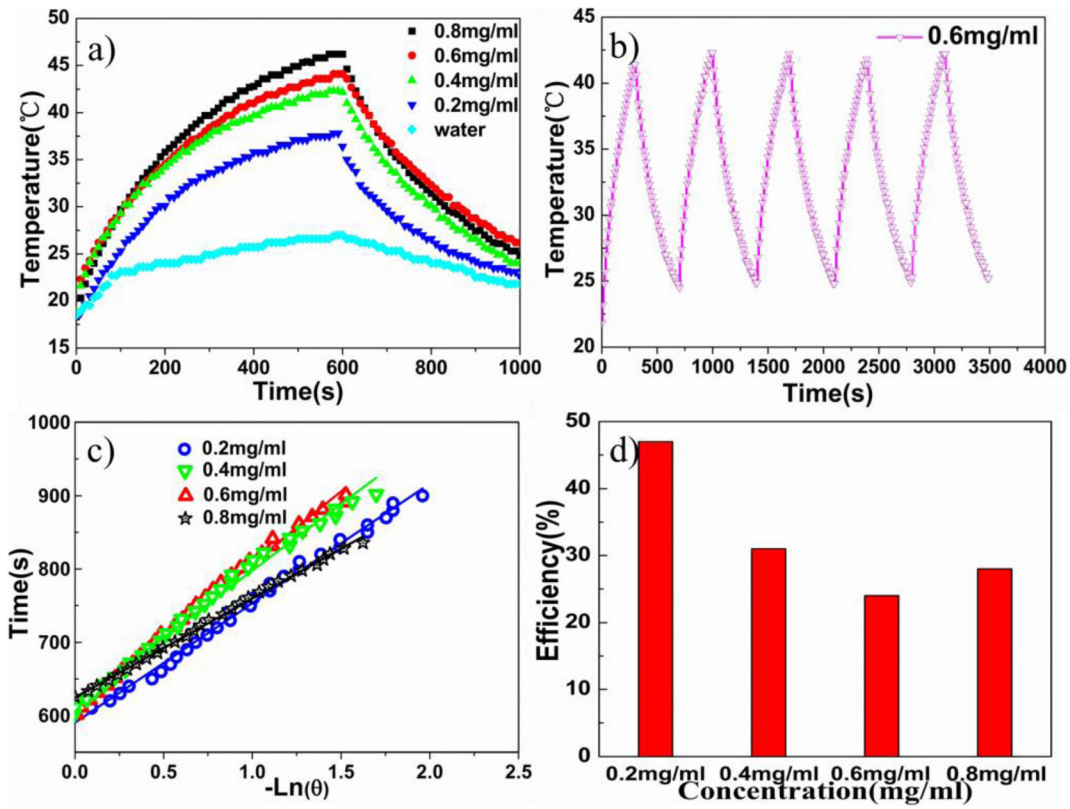

Fig. 5 **a** Photothermal response of pure water and aqueous dispersions with different concentrations of 0.8, 0.6, 0.4, and 0.2 mg/ml. **b** Temperature elevation of $Cu_{2-x}Se$ aqueous dispersions over five ON/OFF cycles of laser irradiation. **c** The heat transfer time constants are calculated. **d** The photothermal conversion efficiencies are calculated

The maximum photothermal conversion efficiency of $Cu_{2-x}Se$ NPs aqueous dispersion can reach to 48% (Fig. 5d). The hollow nanostructures can enhance light absorption through the multiple reflection process in the hollow cavity, resulting in the effective path length increasing for light absorption (Seadira et al. 2017; Sun et al. 2012, 2013). $Cu_{2-x}Se$ nanostructures show also high optical extinction coefficients during the range of NIR wavelength from 650 to 1100 nm and convert the light into considerable heat under photo excitation due to the intense LSPR absorbance (Zhang et al. 2017; Hessel et al. 2011; Zhu et al. 2017).

Conclusions

$Cu_{2-x}Se$ hollow nanoparticles are with potentially applications as photocatalysts and photothermal therapy. $Cu_{2-x}Se$ hollow NPs with a diameter 160–180 nm and a shell thickness 11.3 nm are successfully synthesized through one-pot microwave-assisted method. The formation mechanism of the hollow structure is analyzed based on the energy theory and kinetic process. $Cu_{2-x}Se$ shows a broad light absorption peak that is located in the NIR spectral region. Preliminary photothermal investigation showed that a definitely irradiation power results in an excellent temperature increasing since the $Cu_{2-x}Se$ is able to convert light into heat rapidly. The high photothermal conversion ability is attributed to strong synergistic effect between LSPR and multiplies reelection in the hollow structures. In addition, the photochemical performance also plays an important role during the process of photothermal conversion. Meanwhile, $Cu_{2-x}Se$ hollow nanoparticles possess good thermal stability and high conversion efficiency (48%).

Funding information This work has been supported by the National Natural Science Foundation of China (11674240, 11504261, and 11747158).

Compliance with ethical standards

Conflict of interest The authors declare that they have no conflict of interest.

References

Ahmad R, Nicholson KS, Nawaz Q (2017) Correlation between product purity and process parameters for the synthesis of Cu_2ZnSnS_4 nanoparticles using microwave irradiation. Nano Res 19:238

Bernal MM, Di Pierro A, Novara C, Giorgis F, Mortazavi B, Saracco G, Fina A (2018) Edge-grafted molecular junctions between graphene nanoplatelets: applied chemistry to enhance heat transfer in nanomaterials. Adv Funct Mater 28: 1706954

Chen XQ, Bai Y, Li Z, Wang LZ, Dou SX (2016) Dou ambient synthesis of one−/two-dimensional CuAgSe ternary nanotubes as counter electrodes of quantum-dot-sensitized solar cells. Chem Plus Chem 81:414–420

Chen XQ, Li Z, Bai Y, Sun Q, Wang LZ, Dou SX (2015a) Room-temperature synthesis of $Cu_{2-x}E$ (E=S, Se) nanotubes with hierarchical architecture as high-performance counter electrodes of quantum-dot-sensitized solar cells. Chem Eur J 21: 1055–1063

Chen XQ, Li Z, Dou SX (2015b) Ambient facile synthesis of gram-scale copper selenide nanostructures from commercial copper and selenium powder. Appl Mater Interfaces 7: 13295–13302

Cao HL, Qian XF, Zai JT, Yin J, Zhu ZK (2006) Conversion of Cu_2O nanocrystals into hollow $Cu_{2-x}Se$nanocages with the preservation of morphologies. Chem Commun 43:4548–4550

Chang Y, Teo JJ, Zeng HC (2005) Formation of colloidal CuO nanocrystallites and their spherical aggregation and reductive transformation to hollow Cu_2O nanospheres. Langmuir 21: 1074–1079

Han C, Li Z, Lu GQ, Dou SX (2015) Robust scalable synthesis of surfactant-free thermoelectric metal chalcogenide nanostructures. Nano Energy 15:193–204

Han C, Sun Q, Cheng ZX, Wang JL, Li Z, Lu GQ, Dou SX (2014) Ambient scalable synthesis of surfactant-free thermoelectric CuAgSe nanoparticles with reversible metallic-n-p conductivity transition. J Am Chem Soc 136:17626–17633

Hanus J, Libenska H, Khalakhan I, Kuzminova A, Kylian O, Biederman H (2017) Localized surface plasmon resonance tuning via nanostructured gradient ag surfaces. Mater Lett 192:119–122

Hessel CM, Pattani VP, Rasch M, Panthani MG, Koo B, Tunnell JW, Korgel BA (2011) Copper selenide nanocrystals for photothermal therapy. Nano Lett 11:2560–2566

Ingole PP, Joshi PM, Haram SK (2009) Room temperature synthesis of 1-hexanethiolate capped $Cu_{2-x}Se$ quan-tum dots, in Triton X-100 water-in-oil microemulsions. Colloid Surface A 337:136–140

Jia GZ, Lou WK, Cheng F, Wang XL, Yao JH, Dai N, Lin HQ, Chang K (2015) Excellent photothermal conversion of core/shell CdSe/Bi_2Se_3 quantum dots. Nano Res 8:1443–1453

Jia GZ, Lu XC, Hao BX, Wang XL, Li YM, Yao JH (2013) Kinetic mechanism of ZnO hexagonal single crystal slices on GaN/sapphire by a layer-by-layer growth mode. RSC Adv 3:12826–12830

Jia GZ, Wu ZN, Wang P, Yao JH, Chang K (2016a) Morphological evolution of self-deposition Bi_2Se_3 nanosheets by oxygen plasma treatment. Sci Rep 6:22191

Jia GZ, Zhang Y, Wang P (2016b) Nano-photo-thermal energy drive MoS_2/ZnO nanoheterojunctions growing. Opt Mater Express 6:876–883

Jiang X, Zhang S, Ren F, Chen L, Zeng JF, Zhu M, Cheng ZX, Gao MY, Li Z (2017) Ultra-small magnetic $CuFeSe_2$ ternary nanocrystals for multimodal imaging guided photothermal therapy of cancer. ACS Nano 11:5633–5645

Kong LD, Xing LX, Zhou BQ, Du LF, Shi XY (2017) Dendrimer-modified MoS_2 nanoflakes as a platform for combinational gene silencing and photothermal therapy of tumors. ACS Appl Mater Interfaces 91:5995–16005

Liao XH, Wang H, Zhu JJ, Chen HY (2001) Preparation of Bi_2S_3 nanorods by microwave irradiation. Mater Res Bull 36:1169–1176

Liu X, Law WC, Jeon M, Wang XL, Liu MX, Kim C, Prasad PN, Swihart MT (2013) $Cu_{2-x}Se$ nanocrystals with localized surface plasmon resonance as sensitive contrast agents for in vivo photoacoustic imaging: demonstration of sentinel lymph node mapping. Adv Healthcare Mater 2:952–957

Liu X, Swihart MT (2014) Heavily-doped colloidal semiconductor and metal oxide nanocrystals: an emerging new class of plasmonic nanomaterials. Chem Soc Rev 43:3908–3920

Ni X, He ZZ, Liu X, Jiao QZ, Li HS, Feng CH, Zhao Y (2017) Ionic liquid-assisted solvothermal synthesis of hollow $CoFe_2O_4$ microspheres and their absorbing performances. Mater Lett 193:232–235

Park CH, Yun H, Yang H, Lee J, Kim BJ (2017) Photothermal imaging: fluorescent block copolymer-MoS_2 nanocomposites for real-time photothermal heating and imaging. Adv Funct Mater 27:16044

Rayman MP (2005) Selenium in cancer prevention: a review of the evidence and mechanism of action. P Nutr Soc 64(16):527–542

Seadira T, Sadanandam G, Ntho TA, Lu XJ, Masuku CM, Scurrell M (2017) Hydrogen production from glycerol reforming: conventional and green production. Rev Chem Eng 34: 695–726

Song WZ, Gong JX, Wang YQ, Zhang Y, Zhang HM, Zhang WH, Zhang H, Liu X, Zhang TF, Yin WZ (2016) Gold nanoflowers with mesoporous silica as"nanocarriers for drug release and photothermal therapy in the treatment of oral cancer using near-infrared (NIR) laser light". J Nanopart Res 18:101

Sun ZQ, Liao T, Kim JG, Liu KS, Jiang L, Kim JH, Dou SX (2013) Architecture designed ZnO hollow microspheres with wide-range visible-light photoresponses. J Mater Chem C 1: 6924–6929

Sun JH, Zhang JS, Zhang MW, Antonietti M, Fu XZ, Wang XC (2012) Bioinspired hollow semiconductor nanospheres as photosynthetic nanoparticles. Nat Commun 3:1139

Tsuji M, Hashimoto M, Nishizawa Y, Kubokawa M, Tsuji T (2005) Microwave-assisted synthesis of metallic nanostructures in solution. Cheminform 11:440–452

Wang DQ, Hou C, Meng LJ, Long JG, Jing JG, Dang DF, Fei ZF, Dyson PJ (2017) Stepwise growth of gold coated cancer targeting carbon nanotubes for the precise delivery of doxorubicin combined with photothermal therapy. J Mater Chem B 5:1380–1387

Xu D, Yang LC, Wang Y, Wang GJ, Rensing C, Zheng SX (2018) Proteins enriched in charged amino acids control the formation and stabilization of selenium nanoparticles in Comamonas testosteroni S44. Sci Rep 8:4766

Yin YD, Rioux RM, Erdonmez CK, Hughes S, Somorjai GA, Alivisatos AP (2004) Formation of hollow nanocrystals through the nanoscale Kirkendall effect. Science 304:711–714

Yu L, Yu XY, Lou XW (2018) The design and synthesis of hollow micro-/nanostructures: present and future trends. Adv Mater 30(38):20

Zhang SH, Huang Q, Zhang LJ, Zhang H, Han YB, Sun Q, Cheng ZX, Qin HZ, Dou SX, Li Z (2017) Vacancy engineering of $Cu_{2-x}Se$ nanoparticles with tunable LSPR and magnetism for dual-modal imaging guided photothermal therapy of cancer. Nanoscale 10:3130–3143

Zhang SH, Sun CX, Zeng JF, Sun Q, Wang GL, Wang Y, Wu Y, Dou SX, Gao MY, Li Z (2016) Ambient aqueous synthesis of ultrasmall PEGylated $Cu_{2-x}Se$ nanoparticles as a multifunctional theranostic agent for multimodal imaging guided photothermal therapy of cancer. Adv Mater 28:8927–8936

Zhu DW, Liu MX, Liu X, Liu Y, Prasad PN, Swihart MT (2017) Au-$Cu_{2-x}Se$ heterogeneous nanocrystals for efficient photothermal heating for cancer therapy. Adv Healthc Mater 2:952–957